Design and Construction of a Series of Compact Humanoid Robots and Development of Biped Walk Control Strategies

Takayuki Furuta[1], Yu Okumura, and Ken Tomiyama

Aoyama Gakuin University, 6-16-1, Chitosedai, Setagaya-ku, Tokyo, 157-8852, JAPAN,
`furuta@artemis.me.aoyama.ac.jp` , `yu@artemis.me.aoyama.ac.jp`, `tomiyama@artemis.me.aoyama.ac.jp` ,
WWW home page: `http://www-esys.me.aoyama.ac.jp`

Abstract. Design and construction of compact body humanoid robots and various biped locomotion control strategies implemented onto them in the ESYS humaniod project at the Engineering Systems Laboratory are presented. Design concepts and hardware specifications of the constructed compact size humanoid robots from Mk.1 to Mk.5 are discussed. As for the the biped walk control, four biped locomotion control strategies all of which have various advantages such as versatility, high energy efficiency, smooth loading on hardware, and real-time gait generation, are proposed. 3D biped dynamic walking of the constructed humanods is realized by implementing the proposed biped control strategies onto them. Results of evaluation experiments on the proposed control strategies are reported.

1 Introduction

The design and construction of compact body humanoid robots and four biped locomotion control strategies that are implemented onto them in the ESYS humanoid project at the Engineering Systems Laboratory are presented in this paper.

Various kinds of component technologies are required for humanoid research. Although many of them have been studied individually by many researchers, most results did not include integration of those technologies. Several humanoid platforms are reported [1][2][3][4]. These humanoid robots, however, are not at fully developed stages. Furthermore, there were not many humanoid researchers until after Honda's P2[5]. The project, called "ESYS humanoid project," was commenced in April 1996 at our laboratory within this rather unheralded era for humanoid research. The purposes of this project are to develop and integrate these component technologies, to implement them onto humanoid robots, and to develop practical humanoid robots that can perform various human-like activities. Moreover the project is aimed at solving several problems that are common to many humanoid robots. Although many component technologies such as the real-time robot vision, hybrid behavior control architecture, and control hardware including original CPU-board, have been developed in our laboratory[6][7], we concentrate on mechanical hardware and control strategies in this paper.

The mode of locomotion for humanoids is biped dynamic walk that is inherently unstable. In order to make the biped locomotion stable and perform human-like activities, both robot hardware and walk control strategies are fundamentally important. For example, all and more of the following factors need to be considered in designing a humanoid body: limited torque of actuators at joints in the robot, rigidity of hardware such as main frames, arms, and legs, impulsive loading at landing of legs that can damage hardware, interference among links, weight and ease of handling. On the other hand, walk controller must have the following characteristics: stability in the sense of continued dynamic walk, practicability with starting, stopping and making turns, high energy efficiency, versatility in choosing landing position of the swinging leg which is one of most notable advantages of biped locomotion.

We have established hardware design concepts and control strategies for humanoid robots that can solve these problems and have realized truly human-like walking capability in our humanoids. High rigidity and lightweight have been realized by adopting FRP and later CFRP as the major structural materials. Ease of and safe handling have been the result of making our humanoids small in height at less than 40 cm. We have employed an orthogonalized link mechanism that can help simplify the robot dynamics that is too complicated to study otherwise. Four proposed strategies, on the other hand, fully exploited the hardware design concept in realizing required characteristics. The first strategy, called the biped walking using virtual multiple link inverted pendulum models, has the advantage of not only high energy efficiency but also real-time gait generation capability with high stability due to effective use of gravity [8]. The second strategy, termed as the use of final states of single-leg supporting phase in

gait generation, realizes stable versatile dynamic walk by formulating biped locomotion problem as a boundary value problem in that the final as well as the initial condition is utilized in generating a gait [9]. The third strategy, the stabilization of biped locomotion using double-leg supporting phase, realizes smooth and stable 3D biped dynamic walking using elimination of impulsive loading on hardware and kicking motion in the double-leg supporting phase. Finally, the most recent strategy, the generation of multi-phase gait with inherently ZMP stable feature, integrates three previous control strategies. This control strategy has advantages of freedom in choosing landing positions of the swinging leg in real-time. This makes it possible for humanoid robots to walk over unknown terrain.

In this paper, specifications and design concepts for construction of humanoids in the ESYS humanoid project are discussed. Next, proposed biped control strategies for the humanoid robots are described. Finally, various stable dynamic walk that have been realized by implementing those strategies onto our humanoid robots are reported.

2   Humanoid Robot Hardware

In the ESYS humanoid project, several types of humanoid robots, named Mk.1 to Mk.5, have been designed and constructed for demonstrating the effectives of the proposed control strategies. In this section, design concepts and mechanical specifications of the humanoid robots are described.

2.1   Design Concepts for Humanoid Robots

The basic design concepts of the ESYS humanoids are as follows:

1. To be low cost in constructing a humanoid robot. This is because we aim at making personal humanoid robots.
2. To be safe for both experimental environment and human.
3. To be able to do maintenance on the robot hardware and control systems easily.
4. To be highly expandable on both robot hardware and control systems.
5. To set the center of gravity of the humanoid robot as high as possible to enhance the usage of gravity in 3D biped walking.
6. To orthogonalize and to eliminate offsets of joint axes of the robot to enable us to simplify dynamics of the robot.
7. To mount as much electronic hardware as possible on the humanoid robot. The exceptions are those special hardware such as the robot vision. The external hardware set should be connected to the on-board system via wireless link to maintain autonomy of humanoids.

Because occasional falls of humanoid robots are expected in experiments of biped walking, it is important that the robot is compact in size and light in weight in order not to harm environment nor human. Small robots have other advantages such as the ease of maintenance and small construction costs as well. It is contemplated to place the center of gravity at a rather high location on the body, just like the human physiology, to reduce the control effort for dynamic walk. This is achieved by locating motors at points higher than the joints and drive joints through parallel link mechanisms.

Following these concepts, we were able to demonstrate versatile dynamic walk in our series of robots. This proves the soundness of the above concepts and shows that our approach is in deed a viable one.

2.2   Specifications of Constructed Robots

In this section, specifications and features of the constructed humanoid robots are described. First, the specifications of the humanoid robots, named Mk.1 to Mk.5, are summarized in Table 1.

Specifications of Mk.1 This first biped robot, Mk.1, was designed and constructed in 1996 to evaluate the feasibility of our approach. It was used to test our first control strategy based on a set of multiple-link virtual pendulum models. As such, Mk.1 had only the lower body with a hip and two legs. It had ten degrees-of-freedom (DOFs). A view and the assignment of DOFs of Mk.1 are shown in Fig. 1. The major frame of Mk.1 is made of Fiber Reinforced Plastic (FRP) in order to make Mk.1 light and rigid. A type of servomotors typically used for remote-controlled scale models is adopted as the actuator for Mk.1. All

Table 1. Specifications of Constructed Mk. Series

Name	Mk.1	Mk.2	Mk.3	Mk.4	Mk.5
Degree of Freedoms	10	19	12	23	24
Height [m]	3.25×10^{-1}	3.80×10^{-1}	3.03×10^{-1}	3.63×10^{-1}	3.56×10^{-1}
Leg Length [m]	2.81×10^{-1}	2.29×10^{-1}	2.11×10^{-1}	2.09×10^{-1}	2.02×10^{-1}
Mass[kg]	1.286	2.500	1.400	2.000	1.900
Main Material	FRP	CFRP	CFRP	CFRP	CFRP

joints are driven by the same servomotor with the maximum torque of $\pm 8.0 kgf \cdot cm$. The servomotor actually is a compact assembly of a DC-motor, a potentiometer, and a servo-control unit. Mk.1 does not have a brain on-board. An external host computer called remote-brain [10] controls the walk of robot by constructing walk control commands and send them to the robot via wireless communication link. Mk.1 was able to perform 3D dynamic walking. It is noted that the joint axes are orthogonal but have offsets.
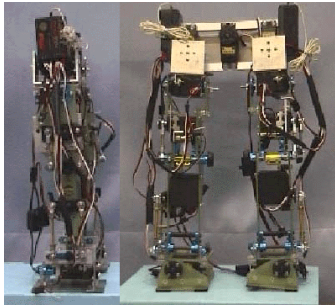

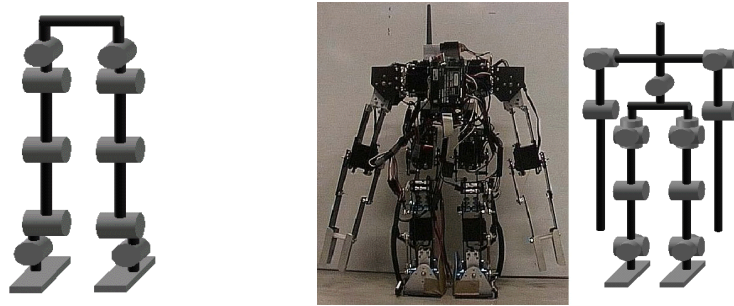Fig. 1. Views and Assignment of DOFs of Mk.1

Fig. 2. A View and Assignment of DOFs of Mk.2

Specifications of Mk.2 The major design concepts of Mk.2 are to eliminate offsets among the axes of joints, to have high rigidity, and to have degrees of freedom in yaw axes in the hip. The assignment of DOFs and a view of Mk.2 are shown in Fig. 2. As is shown in the figure, the axes of joints in the hip and ankles on Mk.2 are orthogonalized and intersects at single points as desired. As we have mentioned, this helps to simplify the formulation of dynamics in the control strategies. Mk.2 is the first humanoid type robot with upper body and arms constructed in the ESYS humanoid project. Carbon Fiber Reinforced Plastics (CFRP) is used as the main construction material for the purpose of higher rigidity. Servomotors with the maximum $\pm 9.5 kgf \cdot cm$ torque are selected for the joints. A wireless modem to send a remote-host computer sensor information is mounted on the robot. The robot, however, does not have the capability of performing dynamic walk but can perform static walk. This is because the lack in both accuracy of the parts and the motor torque, especially in the hip. These findings reinforced the importance of the precision of hardware construction and the spare torque of motors at joints where high loadings are expected. The robot is used mainly as the platform for humanoid behavior controller in such experiments on fall avoidance, standing up from the ground after a fall, and so on. The rather large size for the arms of Mk.2 is actually for this purpose.

Specification and Features of Mk.3 A view and the assignment of DOFs for the biped robot named Mk.3 are shown in Fig. 3. 3D dynamic walk is realized with Mk.3 robot by solving the problems of it's predecessors. Moreover, various type of walk such as starting, stopping, and making turns are realized for the first time in the ESYS humanoid project using this robot. This robot is originally controlled by the method that uses final states of single-leg supporting phase as gait design parameters. The foot print is 6 cm by 7.5 cm. These dimensions are important when we adopt ZMP stability criterion that will be described later. All joints of the robot are equipped with servomotors with the maximum torque of $\pm 9.5 kgf \cdot cm$ and the maximum speed of 11.6 rad/sec. This maximum torque is the same as that of Mk.2 but can provide enough spare torque because of the design change and the lowered torque requirement resulted from the new design. For the purpose of landing the swinging leg smoothly, bottoms of the feet are covered by sorbothine that is a material absorbing impulsive force effectively.

Later, Mk.3 is refined to include a wireless modem and a CCD camera and used for humanoid behavior control study. The modified Mk.2 was able to perform intelligent activities such as finding an object, avoiding it, and kicking a ball [6][7].
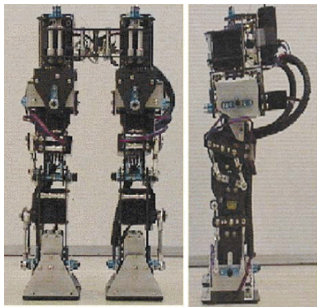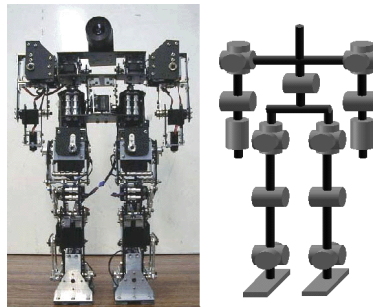
Fig. 3. Views and Assignment of DOFs of Mk.3   Fig. 4. A View and Assignment of DOFs of Mk.4

Specifications and Features of Mk.4 A view and the assignment of DOFs of humanoid robot Mk.4 are shown in Fig. 4. The lower half of the humanoid robot is a refined version of Mk.3 and can perform various 3D biped dynamic walking. The difference is that the operating ranges of joint angles are made larger than those of Mk.3. This gives Mk.4 more versatility in choosing gait and makes it possible, for example, to walk up-stairs. A CCD camera and a wireless modem are mounted on the upper body of Mk.4.

Two walking strategies are implemented on Mk.4. One of them is based on multiple-link virtual inverted pendulum models and the other one on generation of multi-phase gait with inherently ZMP stable feature. Mk.4 is able to perform stable dynamic walking including turn motion, starting, and stopping using both control strategies. It is expected to be able to avoid an obstacle by stepping over it (will be reported elsewhere).

Specifications and Features of Mk.5 The fifth generation humanoid robot, Mk.5, is designed in April 2000 to integrate component technologies developed so far and to test human-like activities on the humanoid body. As such, it has a full body with two arms and a head with two color CCD cameras. Front and side views and the assignment of the DOFs of Mk.5 are shown in Fig. 5. Despite the fact that it has a full body and the full-featured electronics corresponding to the full body, it stands at only 356 mm and is smaller than Mk.4 in Fig. 4. This is because the readily available servomotors do not have enough torque to house all the electronics that are required for humanoid behavior generation. Therefore it is necessary to minimize the size of the robot. The result is a stunning weight of 1.9 kg including the battery. It also has numerous improvements over Mk.4 in hardware configuration. For example, the distance between the two leg axes in the hip is decreased in order to reduce the torque requirement in the hip joints, the length and thickness of leg limbs are all decreased for the same reason. As for the electronic hardware, a battery pack, a wireless modem, sensors such as accelerometer, force sensors, two CCD cameras and so on, and a Sage CPU system are mounted on the robot. The Sage CPU board that constitutes the local brain is designed in the ESYS humanoid project and has a conbination of compact size and high calculation capability with floating point arithmetic. It takes the roles of formulating reference data for biped locomotion, administering information from the sensors, sending and receiving data to and from a remote-host via wireless communication link, and control micro-controllers that are responsible for actuator control and sensor data acquisition. The mico-controllers and SAGE are connected through I^2C serial bus that comprises in-body network. With all this loading, Mk.5 can still be active over 20 minutes by a single charging of the onboard battery.

Mk.5 can perform all the 3D dynamic walk of it's predecessors even better. It can also transfer objects using it's arms. It is a complete humanoid robot platform that can be used for studies of intelligent behaviors of humanoids. It is also mentioned that the construction cost of Mk.5 is less than 6,500 dollars excluding the development cost and the real-time OS.

3   Control Strategies

This section describes the four biped walking strategies developed in the ESYS humanoid project which are applicable to humanoids in general. First, overviews of the control strategies are presented. Next, a controller structure that is the underlying structure of all four proposed control strategies is introduced. Finally, dynamics of the robots and four developed control strategies are discussed in detail.
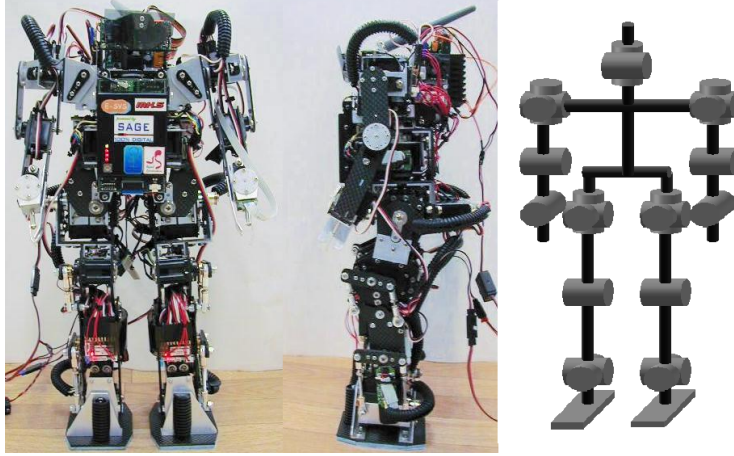
Fig. 5. Views and Assignment of DOFs of Mk. 5

3.1 Overview

Relationships among the four proposed control strategies are shown in Fig. 6. When the ESYS humanoid project commenced in 1996, biped walking using multiple link virtual inverted pendulum models was proposed. It had features such as high energy efficiency and real-time gait generation. This strategy had various essential advantages and had much influence on another proposed strategies. In 1998, the use of final states of single-leg supporting phase in gait generation was proposed and shown to be successful in realizing various dynamic walk. This again became a basis for another strategies proposed later. This strategy realizes freedom of the motion in real-time gait generation which is one of the most useful features of biped locomotion and never realized before. Finally, we proposed the generation of multi-phase gait with inherently ZMP stable feature that integrates two previous strategies and the stabilization of biped locomotion using double-leg supporting phase as a new method that can realize smoother gaits and possibility of avoiding a small obstacle on the ground by stepping over it. The last strategy has provisions for real-time gait adjustment due to the existence of an inherently stable phase in developed gaits.
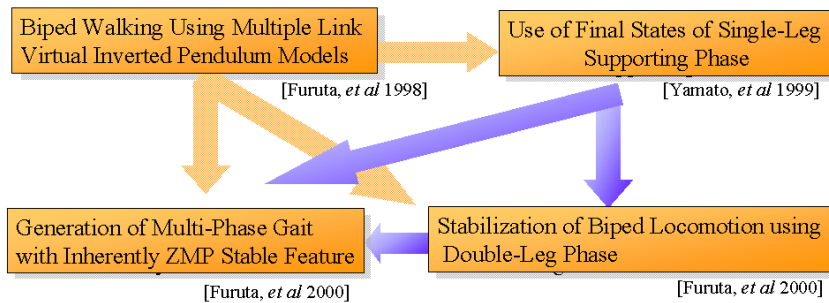

Fig. 6. Overview of Control Strategies in an ESYS Humanoid Project

3.2 Controller

The overview of the controller underlying all of the proposed walk control strategies is shown in Fig. 7.

Simply speaking, all the proposed control strategies calculate reference angles of robot joints when a pattern of the robot's walk is given to them. Then, the computed reference angles are sent to servo controller units with local angle feedback to actuate robot joints. This coordinated actuation of appropriate joints realizes dynamic walking.

3.3 Dynamics

This section describes dynamic models of the constructed robots used in this paper for single-leg supporting phase, double-leg supporting phase, and contacting phase. The most important stability criterion,
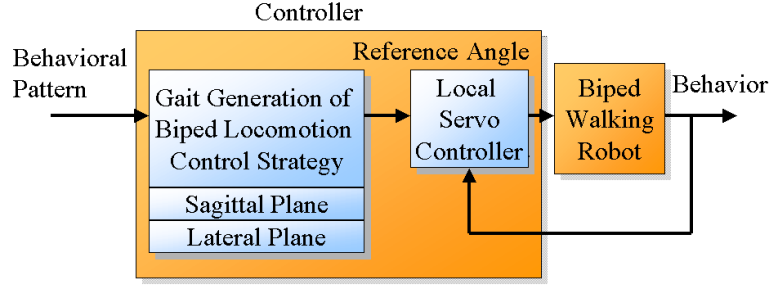
Fig. 7. Schematic Diagram of Walk Controller

called the ZMP criterion, that humanoids must satisfy in order to avoid falls while they are walking is presented. Several assumptions on biped locomotion models are also discussed.

Biped locomotion is a complex process to model. Therefore, we assume that the 3D dynamics can be divided into two separate dynamics in orthogonal planes called the sagittal and lateral plane dynamics as shown in Fig. 8. Here plane dynamics along the yaw axis is not included because it has minimum influence on walk dynamics compared to those by other plane dynamics when the speed of motion is relatively slow. Another assumption is that the two plane dynamics has no interaction with each other. This assumption is justified by the same reason.
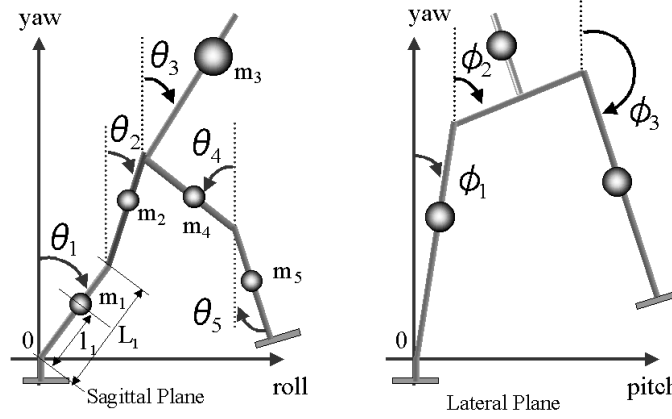

Fig. 8. Models of Robot in Two Planes

Single-Leg Supporting Phase: The equations of motion in both planes are represented by the same form as in Eq. 1.

$$\mathbf{A}(\theta)\ddot{\theta} + \mathbf{b}(\theta, \dot{\theta}) = \mathbf{u}, \tag{1}$$

where $\mathbf{A}$ is the inertial accelerating-related symmetric positive definite matrix, $\mathbf{b}$ is the Coriolis, centrifugal and gravity loading force vector and $\mathbf{u}$ is the generalized torque vector.

Here, a linearized model dynamics for the robot is derived. In Fig. 8, m_i, L_i and l_i denote respectively, the mass, the length and the distance between the mass center and the lower joint of link i. θ_i and τ_i represent the angle and input torque of joint i.

The dynamics of this model can be expressed by the Lagrangian dynamics model given by

$$\mathbf{M}\ddot{\theta} + \mathbf{D}(\dot{\theta}) + \mathbf{G}\theta = \mathbf{u} \tag{2}$$

where

$$\mathbf{M} = \begin{bmatrix} \alpha_1 & \beta_1 & \beta_2 & \beta_3 & \beta_4 \\ \beta_1 & \alpha_2 & \beta_5 & \beta_6 & \beta_7 \\ \beta_2 & \beta_5 & \alpha_3 & 0 & 0 \\ \beta_3 & \beta_6 & 0 & \alpha_4 & \beta_8 \\ \beta_4 & \beta_7 & 0 & \beta_8 & \alpha_5 \end{bmatrix}, D = \begin{bmatrix} D_1 + D_2 & -D_2 & 0 & 0 & 0 \\ -D_2 & D_2 + D_3 & -D_3 & 0 & 0 \\ 0 & -D_3 & D_3 + D_4 & D_4 & 0 \\ 0 & 0 & D_4 & D_4 + D_5 & -D_5 \\ 0 & 0 & 0 & -D_5 & D_5 \end{bmatrix}$$

$$\mathbf{G} = \begin{bmatrix} -\gamma_1 & 0 & 0 & 0 & 0 \\ 0 & -\gamma_2 & 0 & 0 & 0 \\ 0 & 0 & -\gamma_3 & 0 & 0 \\ 0 & 0 & 0 & -\gamma_4 & 0 \\ 0 & 0 & 0 & 0 & -\gamma_5 \end{bmatrix}, \mathbf{u} = \begin{bmatrix} \tau_1 - \tau_2 \\ \tau_2 - \tau_3 \\ \tau_3 + \tau_4 \\ \tau_4 - \tau_5 \\ \tau_5 \end{bmatrix}$$

The definitions of parameters in the above matrix are given in [8]. Note that Eq. 2 is linearized about $\theta = \mathbf{0}$.

Double-Leg Supporting Phase: Development of a model for the double-leg supporting phase is based on the assumption that the bottoms of both feet are fixed to the floor. The degrees of freedom in this phase is reduced by this constraint. By introducing Lagrangian multiplier $\mathbf{\Gamma}$ for a set of constraint forces, the dynamic equation of this phase is derived as follows[11] [12]:

$$\mathbf{A}(\theta)\ddot{\theta} + \mathbf{b}(\theta, \dot{\theta}) = \mathbf{u} + \mathbf{E}(\theta)^T \mathbf{\Gamma}(\theta, \dot{\theta}, \mathbf{u}), \tag{3}$$

where $\mathbf{E}(\theta)$ is the Jacobian matrix and $\mathbf{\Gamma}$ indicates the constraint force given below.

$$\mathbf{\Gamma} = -\left[\mathbf{E}\mathbf{A}^{-1}\mathbf{E}^T\right]^{-1} \left[\dot{\mathbf{E}}\dot{\theta} + \mathbf{E}\mathbf{A}^{-1}\left[\mathbf{u} - \mathbf{b}\right]\right] \tag{4}$$

This equation is the same as that for the single-leg supporting phase except the second term on the right hand side. It is noted that the observation of the direction of this constraint force Γ enables us to determine transitions from the double-leg supporting phase to the single-leg supporting phase.

Contacting Phase: The touchdown of the swinging leg to the floor is modeled as follows on the assumption that the contact is made without bouncing [8].

$$\dot{\theta}^+ = \left[\mathbf{I} - \mathbf{A}^{-1}(\theta)\mathbf{R}(\theta)\mathbf{S}(\theta)\right] \dot{\theta}^-, \tag{5}$$

where R and S are matrices that contain lengths and masses of links and the suffixes $-$ and $+$ indicate before and after the collision, respectively. This model is an algebraic equation and implies that the angular velocities are changed discontinuously during the short duration of the touch down. Note that the joint angles remain unchanged during the collision because of the non-trivial inertia of the legs.

ZMP Criterion As we stated above, these models are based on the assumption that the supporting leg is effectively fixed on the ground. This assumption is essential for stable walk.

Satisfying this assumption and avoiding falls, biped mobile robots must satisfy a stability criterion, called ZMP criterion[5,6], during the motion of walk. This criterion was originally developed by Vukobura-tovic [16] and can be stated as the following: the zero moment point (ZMP) of a biped robot is maintained within the foot print of the supporting leg. For the purpose of studying stability margins, the zero moment point can be represented as follows:

$$X_{ZMP} = \frac{\sum_{i=0}^n m_i x_i(\ddot{y}_i + g) - \sum_{i=0}^n m_i y_i \ddot{x}_i}{\sum_{i=0}^n m_i(\ddot{y}_i + g)} \cong \frac{-\tau_1}{Mg}, \tag{6}$$

where m_i are masses of link-i, x_i and y_i are positions of the masses of link-i and M is the mass of the biped robot. From this equation, the ZMP criterion reduces to a condition on the ankle joint torque τ_1 that τ_1 be small enough so that the above ZMP lies within the foot print. Note that this condition is trivially satisfied if τ_1 is kept at zero. This fact is exploited in a more recent developed walk strategies.

3.4 Control Strategy I: Biped Robots using Multiple Link Virtual Inverted Pendulum Models

In this section, we discuss a method of gait generation using multiple link virtual inverted pendulum models.

Simplified Dynamics Model for Reference Model One of the constraint conditions that simplify the dynamics model of the legs is that some joints are kept fixed. Specifically, we adopt the following constraints: (i) the knee angle for the supporting leg is fixed at a straight line and (ii) the posture of the upper body is kept up-right at $\theta_3 = 0$. Furthermore, we assume that (iii) the torque at the ankle joint is set at zero. We can summarize all those constraint conditions as follows:

$$\text{Constraint 1 } : \tau_1 = 0 \tag{7}$$
$$\text{Constraint 2 } : \theta_2 = \theta_1 \tag{8}$$
$$\text{Constraint 3 } : \theta_3 = 0 \tag{9}$$

Note that Constraint 1 guarantees the ZMP stability.

To further simplify the dynamics equation of the non-supporting leg, the following assumptions for the angles θ_4 and θ_5 are also made.

$$\theta_4 = \theta_1 \tag{10}$$
$$\theta_5 = \theta_4 - \theta_{5s} \sin^2 \left(\frac{\pi}{T} t \right) \tag{11}$$

where T represents the time required for a single step, and θ_{5s} is a design parameter.

The set of equations Eq. 7, Eq. 8, Eq. 9, Eq. 10 and Eq. 11 reduces the model of the legs to a five-link inverted pendulum. Applying those equations to Eq. 2, we can obtain the following differential equation.

$$a \cdot \ddot{\theta}_1 - b \cdot \theta_1 = c - d \cdot sin^2 (e \cdot t) \tag{12}$$

where

$$a = \alpha_1 + \alpha_2 - \alpha_4 - \alpha_5 + 2\beta_1 + \beta_2 + \beta_5 - 2\beta_8$$
$$b = \gamma_1 + \gamma_2 - \gamma_4 - \gamma_5$$
$$c = 2(-\alpha_5 + \beta_4 + \beta_7 - \beta_8) \cdot \theta_{5s} \cdot e^2$$
$$d = 2 \cdot c - \gamma_5 \cdot \theta_{5s} \tag{13}$$
$$e = \frac{\pi}{T} \tag{14}$$

By solving Eq. 12, θ_1 can be expressed by the following equation.

$$\begin{aligned} \theta_1 = K_1 - K_2 \cdot \cos(2et) + C_1 \cdot \exp(K_3 t) \\ + C_2 \exp(-K_3 t) \end{aligned} \tag{15}$$

where

$$C_1 = \frac{1}{2} \left(\theta_{1s} + \frac{1}{K_3} \dot{\theta}_{1s} - K_1 + K_2 \right) \tag{16}$$

$$C_2 = \frac{1}{2} \left(\theta_{1s} - \frac{1}{K_3} \dot{\theta}_{1s} - K_1 + K_2 \right) \tag{17}$$

$$K_1 = \frac{d - 2c}{2b} \tag{18}$$

$$K_2 = \frac{d}{2(b + 4e^2 a)} \tag{19}$$

$$K_3 = \sqrt{\frac{b}{a}} \tag{20}$$

and θ_{1s} represents the initial angle of θ_1. Using Eq. 8, Eq. 9, Eq. 10, Eq. 11 and Eq. 15 as reference angles for θ_2, θ_3, θ_4, θ_5 and θ_1, we can make the apparent friction at the ankle zero. A significant implication of this is that the dynamic walk realized through this method effectively utilizes the gravity. As noted before, the walk trivially satisfies the ZMP stability condition. We call this dynamics as 5-link Virtual Inverted Pendulum. We adopt this as the reference model for our model reference type controller.

Constraint Conditions for Continuous Walking When the robot is in continuous walking, following equations will be satisfied.

$$\theta_{1s} = \sigma \cdot \theta_1(T) \tag{21}$$

$$\sigma > 0 \tag{22}$$

where σ is the parameter of the step length. If σ is larger than 1 then the step length increases. If the step period T is fixed, then $\sigma > 1$ implies that the speed of walking increases. On the other hand, if σ is smaller than 1, it indicates the robot's walking speed is decreased. The robot is in steady continuous walking if σ is set to 1. The above observation can be used to realize starting and stopping of the robot. For example, if we increase σ from 0 to a certain positive value, the robot would start walking from standing still. On the other hand, if we decrease σ from a positive value to zero, then the robot would slow down and stop walking.

Applying Eq. 21 to Eq. 15, a new constraint for the reference angle $\dot{\theta}_{1s}$ given by Eq. 23 is derived.

$$
\begin{aligned}
\dot{\theta}_{1s} &= \frac{(-2\sigma - K_4)\,\theta_{1s} - 2\,(K_1 + K_2) + (K_1 - K_2)\,K_4}{K_5}K_3 \\
&= f_1(\theta_{1s}, T) \\
&\equiv f_2(\epsilon, T) \tag{23}
\end{aligned}
$$

where $K_4 = \exp(K_3 T) + \exp(-K_3 T)$, $K_5 = \exp(K_3 T) - \exp(-K_3 T)$ and ϵ represents the stance for a single step (See Fig. 9) . Note that if the desired ϵ and T are determined, then $\dot{\theta}_{1s}$ is calculated using Eq. 23. In order to achieve the derived initial speed ($\dot{\theta}_1 = \dot{\theta}_{1s}$), the kicking force F defined by Eq. 24 is exerted.

$$F = K_{kick} \cdot \left\{ \dot{\theta}_{1s} - \dot{\theta}_1(0) \right\} \tag{24}$$

At each step, from the desired T_k and ϵ_k, the required initial speed $\dot{\theta}_{1sk}$ and the kicking Force F_k are calculated as Fig. 9 shows.
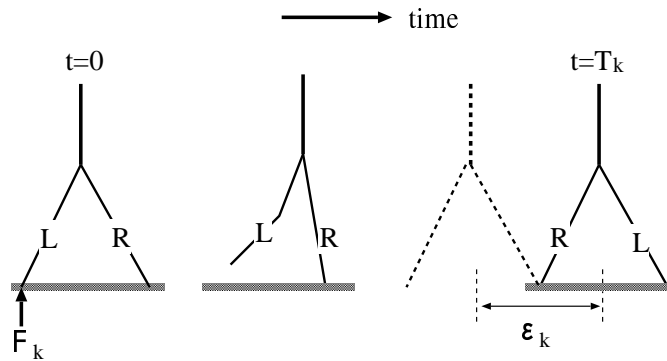

Fig. 9. Scheduling of Robot's Stance at k-th Step

Model Reference Controller using Single Link Virtual Inverted Pendulum for Lateral Plane Dynamics Here again, a model reference type controller with virtual inverted pendulum as a reference model is adopted in lateral plane motion. Consider a one link virtual inverted pendulum model shown in Fig. 10 where M is the mass at the center of gravity, ϕ_i are relative angles of adjacent links, q is the angle of inverted pendulum measured from the vertical line, q_m is the maxmum incline, q_0 denotes the initial angle and L is the length of virtual inverted pendulum model. The motion of this one link virtual inverted pendulum model is given by Eq. 25 through Eq. 28.

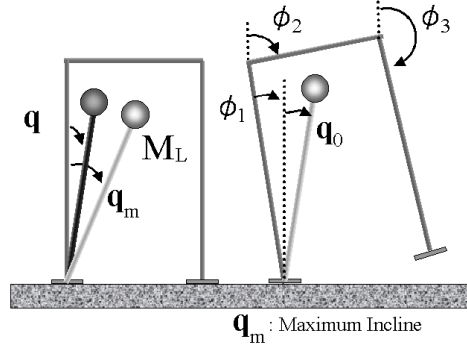$$\phi_1 = q_0 \cosh\left\{ \alpha(t - \frac{T}{2}) \right\} - q_m \tag{25}$$

Fig. 10. Model of Biped Walking Robot for Lateral Motion

$$\phi_2 = \frac{\pi}{2} + \frac{2}{3}\phi_1 \tag{26}$$

$$\phi_3 = \pi + \phi_1 \tag{27}$$

$$\alpha = \sqrt{\frac{g}{L}} \tag{28}$$

Finally, the 3D walking is realized by synchronizing the motions in lateral and sagittal planes using the same time frame for each step $0 \leq t \leq T$.

3.5   Control Strategy II: Use of Final States of Single-Leg Supporting Phase

The discussion in this section is concentrated on a type of biped locomotion that is achieved by neglecting the double-leg supporting phase and assuming smooth level grounds. The method exploits final conditions of a single step in designing a gait.

Trajectory between initial and final state Once both the initial and the final conditions of a single step are given, the trajectories of joint angles between them can be generated using interpolation by polynomials. This method has an advantage that the gait generation using polynomials is computationally cheap and is suited for real-time gait generation. This section justifies the use of trajectories generated by polynomial interpolation by comparing them with those that are optimally generated on the basis of minimum expenditure of control.

A simplified model that is employed for comparison of these trajectories is illustrated in Fig. 11, where
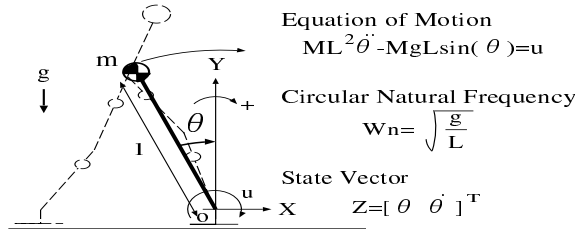

Fig. 11. Inverted Pendulum Model

M is the mass of the robot equivalently located at the center of gravity and L is the length of the virtual inverted pendulum model. First, a trajectory of an angle is assumed to follow a polynomial equation given below.

$$\theta = \alpha_0 + \alpha_1 t + \alpha_2 t^2 + \alpha_3 t^3 \tag{29}$$

The order of this polynomial is chosen to be three because that is necessary and sufficient for specifying angles and angular velocities on both ends. The coefficients α_i are computed by the set of the boundary conditions.

Next, the non-linear model in Fig. 11 is linearized and a standard set of conditions for optimal trajectories, that can be derived using variational technique, are utilized to compute the minimum energy expenditure trajectory between the specified initial and final conditions. Then, the two trajectories are compared and found to agree well for practical cases. The detailed comparisons of trajectories as well as explanations of optimal conditions have been published elsewhere [10] and are omitted here.

This proximity justifies the use of polynomial trajectories instead of minimum energy ones as the reference trajectories for the sake of real-time gait generation.

Based on the above observations, the reference angles for all joints of biped robots are constrained by polynomial equations. Since the initial conditions of a single step is determined by what had happened in the previous step, these conditions are given when a step is initiated and need to be measured. However,the final conditions are yet to be specified and are subject to selection within a reasonable boundary. We constructed a table of ranges for final conditions that guarantee walk stability corresponding to typical initial conditions. Thus the final conditions can be treated as design parameters of gait and the angle trajectories in each step are generated by selecting a set of final states from this prepared states.

Final States in Lateral Plane The motion in Lateral plane is regarded as the stamping motion at a single point. In order to realize the stamping motion for biped robots, this study again utilizes a virtual inverted pendulum model shown in Fig. 12, where M is the mass of the biped robot at the center of gravity and L is the length of the virtual inverted pendulum model.
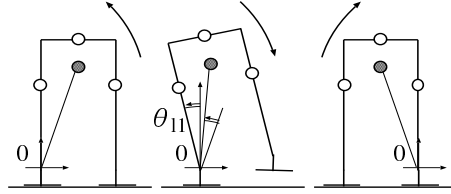

Fig. 12. Model of Biped Robot in Lateral Plane

First, all angles are assumed to be constrained by the polynomials.

$$\theta_{li} = \alpha_{li0} + \alpha_{li1}t + \alpha_{li2}t^2 + \alpha_{li3}t^3 \tag{30}$$

To simplify the computation, we further assume that the hip joint angles are kept at the right angle, namely.

$$\theta_{l2} = \frac{\pi}{2} + \theta_{l1} \tag{31}$$

$$\theta_{l3} = \pi + \theta_{l1} \tag{32}$$

The final state and the time duration for a single step are obtained by the motion of the inverted pendulum. Sets of typical final states obtained by this method are shown in Table 2. The motion in

Table 2. Final States in Lateral Plane

θ_f [deg]	$\dot{\theta_f}$ [deg/sec]
$[-12.5\ 77.5\ 167.5]^T$	$[0\ 0\ 0]^T$
$[0\ 90\ 180]^T$	$[109\ 109\ 109]^T$

Lateral plane is generated by choosing a final state from these states. Figure 13 shows an angle trajectory of the supporting leg in a stamping motion. The angle trajectory from T=2.6 sec to T=4.4 sec represents the stamping motion for three steps.

The ZMP trajectory in the Lateral plane for a single step is shown in Fig. 14. From this figure, we can conclude that the width of the robot foot must be at least 3 cm. Since Mk.3 has the foot print of 6 cm by 7.5 cm, it can be concluded that a stable stamping motion is realized.
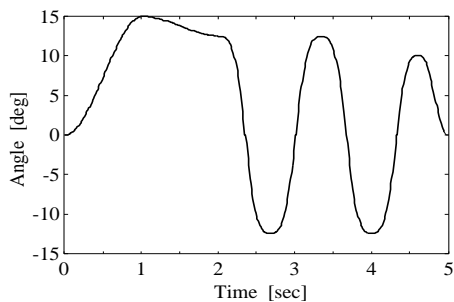
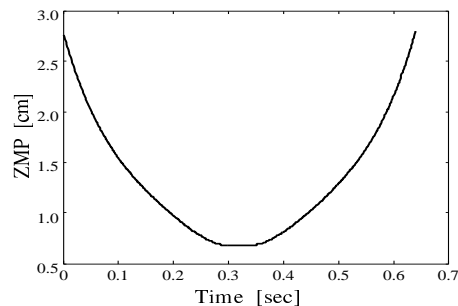Fig. 13. : Angle Trajectory of Supporting Leg

Fig. 14. : ZMP Trajectory in Lateral Plane

Final States and Gaits in Sagittal Plane In the same way as the Lateral plane, motion of all joints in Sagittal plane are constrained by polynomial equations.

$$\theta_{si} = \alpha_{si0} + \alpha_{si1}t + \alpha_{si2}t^2 + \alpha_{si3}t^3 \tag{33}$$

A typical set of pre-chosen final states that are acquired by numerical simulations is shown in Table. 3.

Table 3. Final States in Sagittal Plane

step length [mm]	θ_f [deg]	$\dot\theta_f$ [deg/sec]
11	$[2\ 1\ 0\ 177\ 179]^T$	$[20\ 20\ 0\ 20\ 20]^T$
34	$[10\ 5\ 0\ 175\ 178]^T$	$[50\ 50\ 0\ 50\ 50]^T$
54	$[15\ 8\ 0\ 173\ 176]^T$	$[70\ 70\ 0\ 70\ 70]^T$

(a) First Step   (b) Steady Walk   (c) Final Step
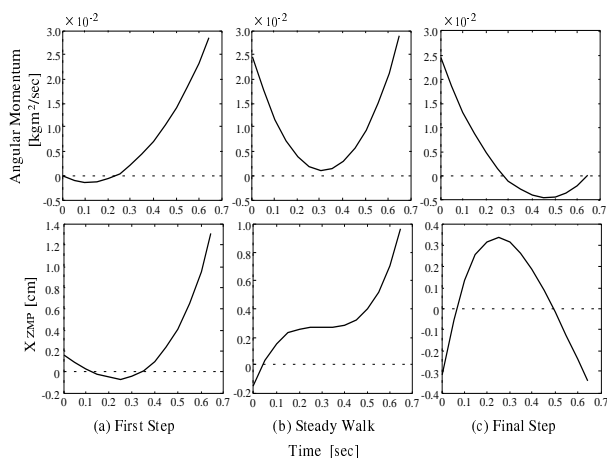Time [sec]

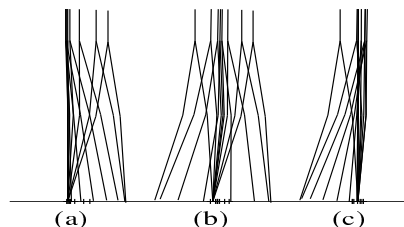Fig. 15. Angular Momentum and ZMP

Fig. 16. Starting and Stopping of Robot

Figure 16 and 15 exemplify biped locomotion including starting and stopping of dynamic walk. In both figures, (a) and (c) indicate starting and stopping of the robot while (b) represents a single step during steady walk with 34 mm step length. The orbits of the angular momentum in Fig. 15 imply that smooth and stable transient gait are successfully generated by the utilization of the final states. Furthermore, it can be concluded from ZMP trajectories that the foot length of 3 cm from the heel to toe is needed for stable walk and that stable walk is realized because actual dimension is 7.5 cm as stated before.

3.6   Control Strategy III: Stabilization of Biped Locomotion using Double-Leg Supporting Phase

This section discusses gait generation in double-leg supporting phase and stabilization of biped locomotion using this double-leg supporting phase.

Models for gait generation in double-leg supporting phase Here, the double-leg supporting phase is modeled by a single-link pendulum shown in Fig. 18. Notable feature is that the pendulum is supported by much larger polygon consisting of a convex hull of two feet than the single foot in the single-leg supporting phase. This phase is therefore almost automatically stable according to the ZMP criterion. This opens up a possibility of using the torque in ankle joints for generating initial states for the single-leg supporting phase of the following step. In this control strategy, desired initial states are achieved by varying the length of the virtual pendulum in this phase. The desired initial states are determined to provide at least the required velocity at various joints.

Initial Conditions: $\theta_{dr(0)}$, $\dot{\theta}_{dr(0)}$
Final Conditions: $\theta_{dr(Td)}$, $\dot{\theta}_{dr(Td)}$

$\theta_{dr(0)}$
$\dot{\theta}_{dr(0)}$

$\theta_{dr(Td)}$
$\dot{\theta}_{dr(Td)}$

$\theta_{dr(0)}$
$\dot{\theta}_{dr(0)}$

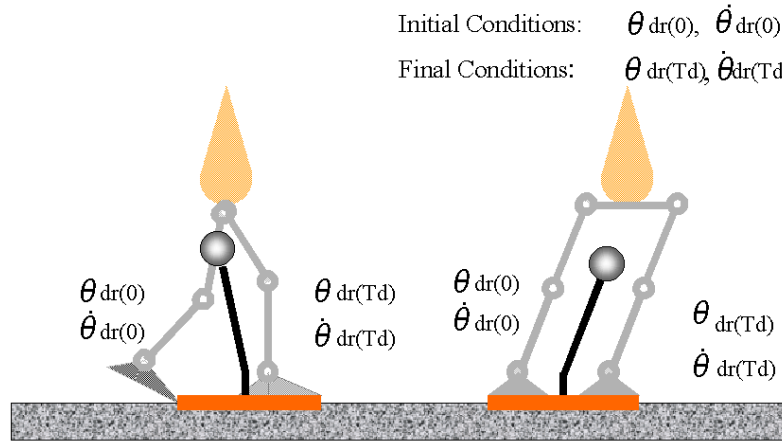$\theta_{dr(Td)}$
$\dot{\theta}_{dr(Td)}$

Fig. 17. Double-leg Supporting Phase Models

Determination of independent joints The dynamics of the double-leg supporting phase need to be derived under the closed-loop link assumption. Therefore the number of joints on which angle trajectories can be generated independently is severely reduced. We must choose those joints on which angle trajectories are first computed. We decided to choose those joints whose trajectories represent the type and characteristics of gait well. Angle trajectories for the chosen joints are independently generated and those of all other joints are derived from them except at singular conditions where more joint trajectories need to be independently generated.

Gait generation for independent joints For the gait generation during the double-leg supporting phase of the independent joints that are chosen as explained above, the method of gait generation using the third order polynomial proposed in Sec. 3.5 is adopted. This method gives the freedom of choosing the final states of the double-leg supporting phase and that states correspond to the initial states of the following single-leg supporting phase.

   In concluding this section, it is emphasized that this control strategy significantly enhances stability of biped locomotion.

3.7   Control Strategy IV: Generation of Multi-Phase Gait with Inherently ZMP Stable Feature

The control strategy described in this section integrates advantages of previous three strategies. Overview of this strategy, gait generation in single-leg and double-leg supporting phases, and the adjustment of angular momentum, which is an essential element for this strategy, are discussed.

Overview of the strategy In Control Strategy IV, a single step of walk is divided into four phases shown in Fig. 18. Those four phases are defined as follows:

– Phase I: Accelerating phase in double-leg supporting phase
   Initial states of the next phase that are necessary to go over to the third phase are generated using angular acceleration in this phase. The energy expenditure in the next phase can be made minimal because of the acceleration in this phase. This accelerating phase is the most stable phase.
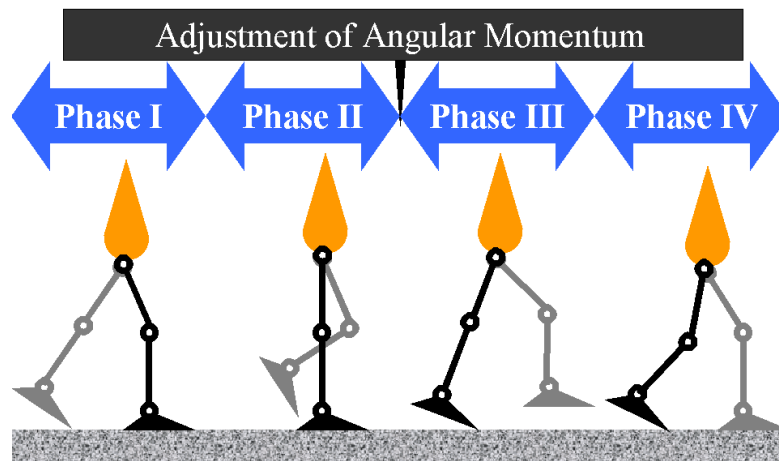
Fig. 18. Gait Phase

  – Phase II: Sole supporting phase in single-leg supporting phase
    Sole supporting phase is one of the single-leg supporting phases. The ankle joint in the supporting leg is free during this phase.
  – Phase III: Toe supporting phase in single-leg supporting phase
    The most epoch-making feature of this control strategy is to take this phase explicitly into consideration. The fact is that this phase is inherently ZMP- stable. This is because ZMP is inherently constrained at the toe of the supporting leg in this phase. This gives an advantage of freely choosing landing positions of the swinging leg in real-time. Exploiting this advantage makes it possible to walk over uneven grounds. At the end of this phase, the robot shifts into the next phase after composing a landing posture.
  – Phase IV: Shock absorbing phase in double-leg supporting phase
    Using ankle, knee, and hip joints, landing impact is absorbed in this phase. This shock absorbing phase is the last phase and a new Phase I starts after this.

This division is based on data from clinical physiology and each phase is identified with a particular function of walk. By considering explicit gait generation for those four phases separately, we can generate versatile gait suitable for realistic terrain.

It is mentioned that the concept of Phase III had never been explicitly considered by biped locomotion researchers. The idea that ZMP must lie within the foot print has been treated as a bible in most biped locomotion studies. This phase is realized in this strategy by projecting the virtual ZMP beyond the front end of the supporting foot. The controller can generate much freer motions that become possible through not constrained by the ZMP criterion.

Gait Generation for Single-leg Supporting Phases (Sole and Toe) This subsection describes gait generation in two single-leg supporting phases (sole and toe). The adopted concepts of gait generation here is the following:

  1. The humanoid is approximately modeled as a single link pendulum in the single-leg supporting phase.
  2. Transition from the sole supporting phase to the toe supporting phase is forced by locking the motion on the ankle joint in the supporting leg. This locking implies that ZMP is thrown forward out of the foot print. The robot motion after the locking can be considered as that of falling forward.
  3. We consider the transition from the sole to the toe supporting phases as a non-elastic collision phenomenon.
  4. As quantities to be controlled, ZMP is available in sole supporting phase while only angular momentum is available in the toe supporting phase.
  5. Landing postures are formed before the transition to the double-leg supporting phase.
  6. Gait is generated using the third order polynomial described in Sec. 3.5.

Various motions and landing positions of the swinging leg in the toe supporting phase are limited by the final state of the sole supporting phase where the states in this phase is the angular velocity around the ankle joint of the supporting leg. This is because the motion in the toe supporting phase is a free

motion without control. The angular velocity is therefore determined in such a way that the desired motion is realized. Therefore, adjustment of angular momentum in the sole supporting phase and the accelerating phase is necessary. This adjustment of angular momentum is discussed later.

Gait Generation for Double-leg Supporting Phases (Accelerating and Shock absorbing) Since the gait in these phases are generated essentially by the method shown in Sec. 3.6, the discussing concentrated on the new feature of angular momentum adjustment.

Adjustment of Angular Momentum In order to give freedom of motions in the toe supporting phase which is inherently ZMP stable, an adequate angular momentum around the ankle joint in the supporting leg must be generated in the sole supporting phase and the accelerating phase. There must be a range of the generated angular momentum for stable continuous walk. If it is too large the robot would tumble forward and if too small the transition to the toe supporting phase would be prevented. The upper and lower limit on the angular momentum are derived using non-elastic contacting model shown in Fig. 19 .
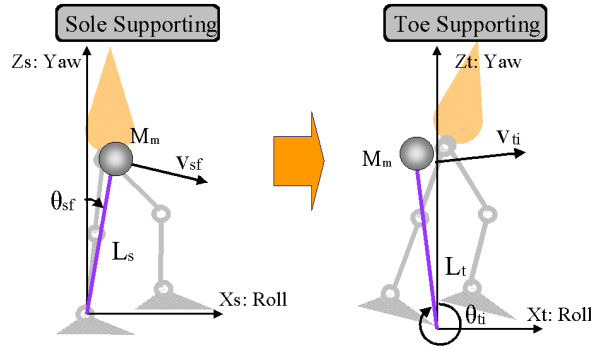

Fig. 19. Model of Virtual Pendulum

– Lower limit on angular momentum The lower limit of the angular momentum is derived from the equations of energy on a one-link model shown in Fig. 19. The equations of energy is given by Eq. 34

$$\frac{1}{2}M_m \left(L_t \dot{\theta}_{ti} \right)^2 + M_m g L_t \cos \theta_{ti} > M_m g L_t + E_m \tag{34}$$

where $\theta_{ti}, \dot{\theta}_{ti}$ are the initial angle and initial angular velocity in the toe supporting phase, M_m and L_t are the total mass and the length of the inverted pendulum, and E_m is the total energy when the mass of the inverted pendulum is at it's highest point.

The equation for the transition from the sole supporting phase to the toe supporting phase on the angular velocity yields

$$\dot{\theta}_{ti} = \frac{L_s}{L_t} \cos(\theta_{ti} - \theta_{sf})\dot{\theta}_{sf} \tag{35}$$

where $\theta_{sf}, \dot{\theta}_{sf}$ are the final angle and final angular velocity in the sole supporting phase.

The lower limit is derived from Eq. 34 and Eq. 35 as

$$\dot{\theta}_{sf} > \frac{\sqrt{2\left\{ gL_t(1 - \cos\theta_{ti}) + \frac{E_m}{M_m} \right\}}}{L_s \cos(\theta_{ti} - \theta_{sf})} \tag{36}$$

where

$$\theta_{sf} = \tan^{-1}\left(\frac{z_g \tan\theta_{ti} + d}{z_g - h} \right) \tag{37}$$

– Upper limit on angular momentum

The upper limit on the angular momentum in the sole supporting phase is derived from the equations of motion of the inverted pendulum model. If the momentum is too large, the robot would jump off the floor and this would be indicated by the fact that the model would predict the reaction force from the floor that is larger than the gravitational force. This is used to derive the upper bound in the momentum below.

$$\frac{v^2}{L_t} < g \qquad (38)$$

where v is the velocity of mass. Equation 38 and Eq. 36 yield

$$\dot{\theta}_s < \sqrt{\frac{g}{L_s}} \ , \qquad \left(L_s \cos^2(\theta_s - \theta_t) \leq L_t \right) \qquad (39)$$

$$\dot{\theta}_t < \frac{\sqrt{gL_t}}{L_s \cos(\theta_s - \theta_t)} \ , \left(L_s \cos^2(\theta_s - \theta_t) > L_t \right) \qquad (40)$$

This indicates the upper limit on the angular momentum.

Following these results, the angular momentum is controlled between the limits to perform stable biped walk.

4 Evaluation Experiments

The results of the experiments to evaluate the presented control strategies are presented in this section.

4.1 Control Strategy I: Biped Robots using Multiple Link Virtual Inverted Pendulum Models

To show the capability of the dynamic walk controller, it is tested with the biped robot Mk.3. The proposed walking controller is implemented on Mk.3 with various parameter sets. It is found that the controller is capable of realizing intended dynamic walk as shown in Fig. 20 where the ZMP locus on the floor of the robot's straight walk is plotted.

From Fig. 20, ZMP for the single-leg supporting phase exists within the region of -30 to 30 mm in sagittal plane and 0 to 20 mm in lateral plane. Since the robot sole is 60x75 mm in size, it is demonstrated that the proposed controller successfully realized stabile biped walk.

The ZMP history in sagittal plane is plotted in Fig. 21, where the broken line is the ideal ZMP trajectory that is calculated from off- line simulations. The solid-line shows the experimental result. This result indicates that although this controller realized stable dynamic walk, there is approximately 100 msec time delay. This is due to the fact that it is controlled by the remote brain through wireless communication and that induces non-trivial time delay. It is not a problem here because the robot is operated open-loop, but will be an issue when the loop is closed by a sensor feedback.
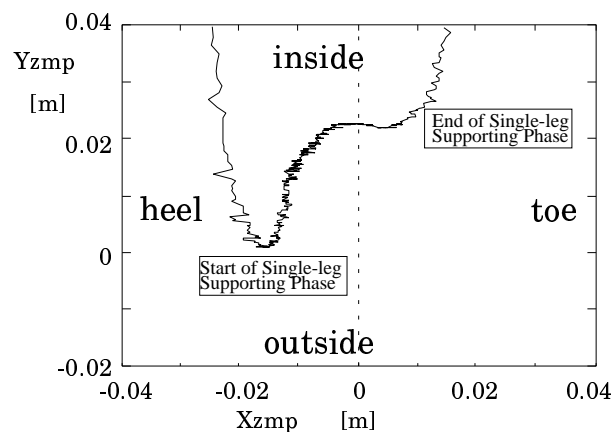

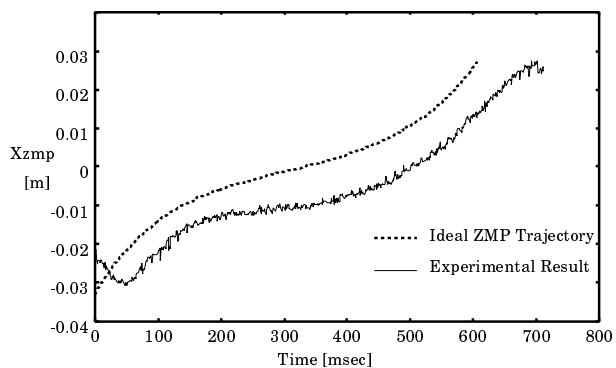Fig. 20. ZMP Locus of Straight Walking Motion

Fig. 21. ZMP Trajectory on Sagittal Plane

   This controller is also used with the Mk.5 robot to realize various dynamic walk. A series of views of startup, forward acceleration, steady walk, deceleration and stopping with 0.7 sec walk period is shown in Fig.22. The maximum step length of Mk.5 is 50 mm.

Fig. 22. Realized Dynamic Biped Locomotion

4.2   Control Strategy II: Use of Final States of Single Supporting Phase

Mk. 3 is commanded to walk using the gait generated in Sec. 3.5. Figure 23 indicates a comparison of the theoretical and measured trajectories of the angular momentum. The figure includes the starting and stopping of the biped robot.
   Figure 24 shows angular momentum and ZMP trajectories over a single step with 0.6 sec walk period and step lengths of (a) 11 mm, (b) 34 mm and (c) 53 mm. This result clearly indicate the capability of this control strategy in generating different walk lengths by changing the final states.

4.3   Control Strategy III: Stabilization of Biped Locomotion using Double-Leg Supporting Phase

The control strategy shown in Sec. 3.6 was applied to the Mk.4 robot. The robot is commanded to do stamping and the resulting ZMP in lateral plane are plotted on Fig. 25. In the figure, (a) is with the method presented in Sec. 3.4 that does not have double-leg supporting phase and (b) is the current control strategy with the double-leg supporting phase. These results indicate the realization of shock absorbing motion with the current startegy using the double-leg supporting phase.

4.4   Control Strategy IV: Generation of Multi-Phase Gait with Inherently ZMP Stable Feature

The control strategy is implemented on the Mk.4 robot and trajectories of ZMP and angular momentum are observed. Typical ZMP and angular momentum trajectories in a single-leg supporting phase are plotted in Fig. 26 where solid and broken curves are experimental and theoretical data. Note that transition from the sole supporting phase to the toe supporting phase occurs at 0.45 sec. In the experiment, the step length is abruptly changed from 60 mm to 80 mm in the middle of the toe supporting phase and this is
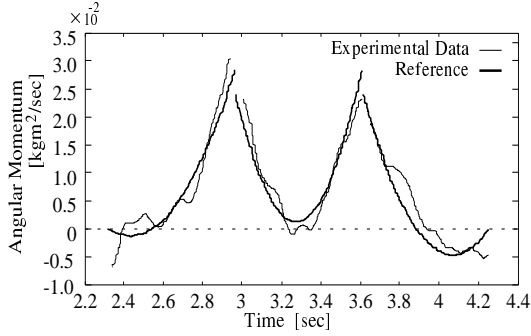
18

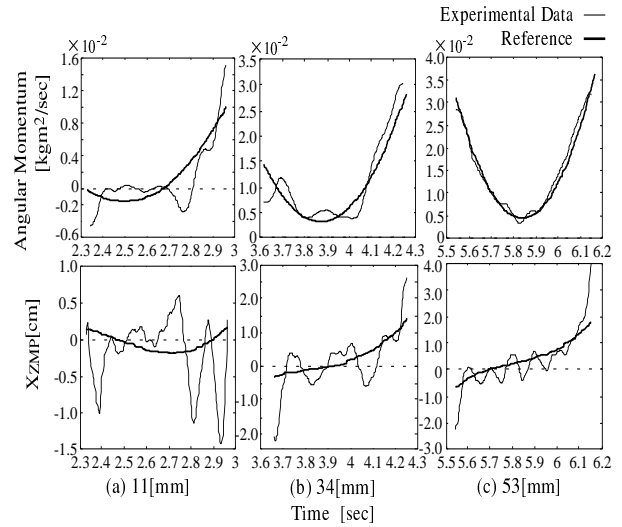Fig. 23. : Starting and Stopping of Robot

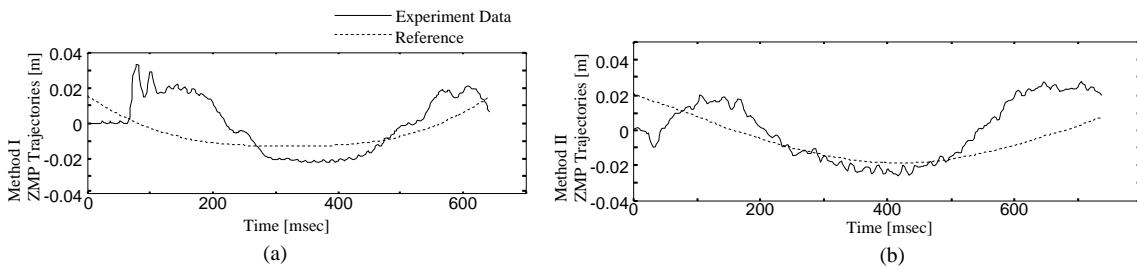Fig. 24. : Angular Momentum and ZMP

Fig. 25. ZMP Trajectories in Lateral Plane

indicated by the two hunches of the theoretical curve in the toe supporting phase in (b). The horizontal dotted line in (b) indicates the lower limit of the angular momentum that is necessary for continuous walk. The experimental result shows the transition taking place above this line and confirms continuous walk. It is also noted that the angular momentum is kept positive in the experiment and that implies the forward motion during the single-leg supporting phase.
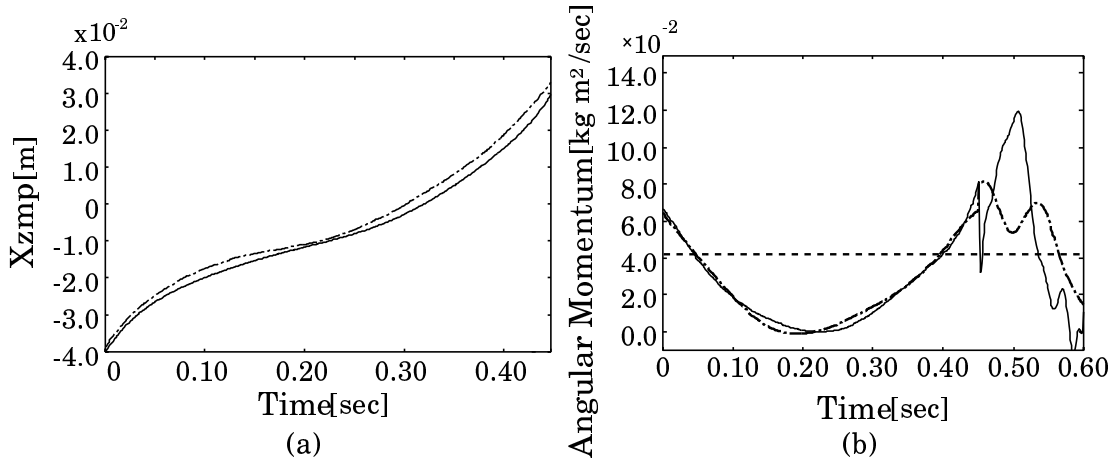

Fig. 26. ZMP and Angular Momentum

5   Concluding Remarks

In this paper, design and construction of five humanoid robots and development of four biped control strategies in the ESYS humanoid project are reported. It is the goal of this project to develop a set of technologies that are necessary to builds sound humanoid research activities. The fundamental policies in designing hardware aspects of humanoids that can contribute in realizing the above goal are stated. With

the realization of the fact that dynamic biped walk is the most fundamental capability of humanoids, four control strategies are developed and explained here. Versatile 3D biped dynamic walk such as starting, stopping, accelerating, decelerating, and making turns are realized using those control strategies. Experimental results that support our claim are also reported in this paper. Mk.5, the most recent robot, has the potential to be a standard platform for humanoid research and is actively used in behavior generation study.

It is noted that other aspects of humanoids such as vision, autonomous behavior generation, and electronic hardware including the original CPU board and in- body network are reported elsewhere.

References

1. M. Kim, S. Kang and S. Lee. "Design and Control of a Humanoid Robot CENTAUR," Proceedings of the Second International Symposium on HUmanoid RObots, pp. 96-101, 1999.
2. T. Morita, H. Iwata and S. Sugano. "Total Design of Body Mechnism for Realizing Human-Robot Symbiosis," Proceedings of the Second International Symposium on HUmanoid RObots, pp. 181-186, 1999.
3. K. Tanie. "MITI's Humanoid Robotics Project," Proceedings of the Second International Symposium on HUmanoid RObots, pp. 71-76, 1999.
4. H. Inoue. "A Platform-based Humanoid Robotics Project," Proceedings of IARP First International Workship on Humanoid and Human Friendly Robotics, pp. I-1-1-4, 1998.
5. K. Hirai et al. "The Development of Humanoid Robot," Proceedings of the 1998 IEEE International Conference on Robotics and Automation, pp. 1321-1326, 1998.
6. M. Shimizu, T. Furuta and K. Tomiyama. "Distributed Behavior Arbitration Network: An Autonomous Behavior Control Architecture for Humanoids," Proceedings of Humanoids 2000, 2000.
7. M. Shimizu, T. Furuta and K. Tomiyama. "Distributed Behavior Arbitration Network: An Autonomous Control Architecture for Humanoid Robots," Proceedings of International Symposium on Micromechatronics and Human Science, pp. 267-274, 1999.
8. T. Furuta et al. "Biped Walking Using Five-link Virtural Inverted Pendulum Model," Asian Control Conference, Vol. 2, pp. 515-517, 1997.
9. T. Furuta et al. "A Stabilization of Biped Locomotion -Use of Final States as Design Parameters," Proceedings of 4th Japan-France/2nd Asia-Europe Congress on Mechatronics, Vol. 1, pp. 348-352, 1998.
10. M. Inaba. Remote-Brained Robotics: Interfacing AI with Real World Behaviors, Robotics Research (T. Kanade and R. Paul, Editors) , The International Foundation for Robotcs Research, Vol. 6, pp. 335–344, 1994.
11. I. Shimoyama et al. "Dynamic Walking of Stilts Type Biped Walking Robot," Transactions of the Japan Society of Mechanical Engineers, Vol. 48, No. 433, pp. 1445-1455, 1983.
12. J. Furusho and A. Sano. "Sensor-Based Control of a Nine-Link Biped," International Journal of Robotics Research, Vol. 9, No. 2, pp. 83-98, 1990.
13. K. Mitobe et al. "Nonlinear Feedback Control of a Biped Walking Robots," Journal of the Robotics Society of Japan, Vol. 14, No. 8, pp. 1194-1199, 1996.
14. H. Minakata and Y. Hori. "Development of Biped Bike Prototype Ostrich-I&II," Proceedings of the 2nd Asian Control Conference, Vol. 3, pp. 319-322, 1997.
15. S. Kajita and K. Tanie. "Study of Dynamic Walk Control of a Biped Robot on Rugged Terrain," Journal of Robotic and Mechatronics, Vol. 5, No. 6, pp. 516-522, 1993.
16. M.Vukobratovic et al. "On the Stability of Biped Locomotion," IEEE Transactions on Bio-Mechanical Engineering, Vol. BME-17, No. 1, pp. 25-36, 1970.
17. A. Takanishi et al. "The Realization of Dynamic Walking by the Biped Walking Robot WL-10RD," Journal of the Robotics Society of Japan, Vol. 3, No. 4, pp. 325-336, 1985.
18. H. Hemami and B.F. Wyman. "Modeling and Control of Constrained Dynamic System with Application to Biped Locomotion in the Frontal Plane," IEEE Transactions on Automatic Control, Vol. AC-24, No. 4, pp. 526-535, 1979.
19. C.L. Golliday and H. Hemami. "An Approach to Analyzing Biped Locomotion Controls," IEEE Transactions on Automatic Control, Vol. AC-12, No. 6, pp. 963-972, 1977.
20. H.Hemami and R.L.Farnsworth. "Postural and Gait Stability of a Planar Five Link Biped by Simulation ," IEEE Transactions on Automatic Control, Vol. AC-22, Vol. 3, pp. 452–458, 1977.